Version of Record: https://www.sciencedirect.com/science/article/pii/S0360544221002401
Manuscript_9581370bbc1aa442f850ba790023f725

Linear electromagnetic energy harvester system embedded on a vehicle suspension: from modeling to performance analysis

B. Lafarge[1], S. Grondel[2], C. Delebarre[2], O. Curea[3] and C. Richard[4]

Abstract—**Although linear electromagnetic energy harvester (LEH) is a promising technique for converting energy in a vehicle suspension, due to the large displacements, one of the main drawbacks of the solutions inside the vehicle is still their size and complexity. To address this issue, this paper focuses on the design and fabrication of a fully embedded LEH without any modification of the suspension initial structure. After a determination of the electrical, mechanical and electromechanical parameters using a Finite Element analysis, the dynamic efficiency is highlighted with a global Bond Graph model. This formalism is well adapted to simulate energy transfers inside multiphysic systems and to reduce the computational time, whereas the finite element model is not exploitable for a complete suspension simulation. In order to validate the Bond Graph simulation results, an embedded prototype has been built and tested in a laboratory environment. The embedded LEH system delivers around 10 watts for a solicitation of linear velocity of 1m/s which is sufficient to power a classical electronic circuit which is in good correlation with the measured ones and significant power has been obtained.**

***Index Terms*—Energy harvesting, car suspension, electromagnetic harvesters, Bond Graph modeling.**

I. NOMENCLATURE

B	magnetic induction, T
C_{fluid}	damping of the shock absorber or the suspension, Ns/m
e	electromotive force, V
E	measured energy E for a full cycle, J
F	integral of the magnetic force for a full cycle, N
F_{damper}	damper force, N
$F_{ext_{touth}}$	generated force by the external tooth, N
F_{mag}	magnetic force, N
F_{mag_i}	magnetic force for coil according to the index i, N
$F_{mag_{totale}}$	total magnetic force, N
F_{mean}	mean force for a full cycle, N
F_{tire}	tire force, N
$i = 1\ to\ 3$	index i indicates the number of considered coils, $dimensionless\ variable$
$i(t)$	current in the coils, A
I	BG storage element I represents the inductance L_{coil_i} of each coil respectively
K_{spring}	stiffness of the suspension, N/m
K_{tire}	tire stiffness, N/m
L_{coil}	coil inductance, H
L_{coil_i}	coil inductance according to the index i, H
M_{sm}	sprung mass, kg
M_{total}	mass is shared between the sprung mass and the unsprung mass of the suspension, kg
M_{usm}	unsprung mass, kg
MGY	power exchange between the electrical and mechanical subsystems of each coil is represented by the modulated gyrator MGY whose the modulation ratio corresponds to the non-linear function $r_i\left(y_p(t)\right)$
N_{coil}	number of the turns contained in a coil, $dimensionless\ variable$
P	maximum power for a full cycle, W
r	non-linear term, $dimensionless\ variable$
r_i	non-linear term according to the index i, $dimensionless\ variable$
R	Bond Graph (BG) dissipative element R represents the resistance R_{coil_i} of each coil respectively

LEH: linear electromagnetic energy harvester

R_{coil}	resistance of the coil, Ω
R_{coil_i}	resistance of the coil according to the index *i,* Ω
R_{load}	resistance of the load, Ω
$V(t)$	voltage at the outputs of the electromagnetic element and of the load circuit, V
$\dot{y}$	linear velocity according to the mechanical variable used on BG, m/s
$y_i(t)$	displacement imposed on the shock absorber, m
$y_1(t)$	unsprung mass displacement, m
$\dot{y}_1(t)$	unsprung mass translation velocity, m/s
$y_2(t)$	sprung mass displacement, m
$\dot{y}_2(t)$	sprung mass translation velocity, m/s
$y_p(t)$	displacement of the electromagnetic harvester with respect to the magnet, m
$\dot{y}_p(t)$	translation velocity, m/s

Greek

Δx	travel distance for a half cycle machine, m
Δt	travel time for a full cycle machine, s
η	electromagnetic efficiency, $dimensionless$
n_{coil_i}	number of turns in a coil according to the index i, $dimensionless\ variable$
ϕ	magnetic induction flux circulating in a coil, Wb

II. Introduction

TODAY energy efficiency is a major concern in the automotive industry which leads also several researches to be developed on energy harvesting in vehicle suspension. In the literature, electro-mechanical conversion applied to vehicle may be realized using different kinds of harvesters [**1**, **2**]: electromagnetic, electrostatic, piezoelectric, Peltier effect and photovoltaic. In theory, mechanical energy conversion can be performed on all links and on all flexible and rigid elements of the suspension [**3**] but the choice regarding the location of the energy harvester and the conversion technology has therefore to be made according to the amplitude of the available movement without disturbing mechanical behavior of the system. As in a car, a portion of the energy dissipated in the form of heat relies directly on the piston movement in the damper's body of the suspension, the authors have decided to focus on converting the dissipated energy in traditional hydraulic shock absorbers.

Several types of energy harvester have already been fixed or embedded into the body of a shock absorber. These solutions can be grouped into two categories [**1**]: the linear harvesters (direct energy harvesters) and the rotary harvesters (indirect energy harvesters). As seen in **Fig. 1**, all techniques convert large displacements with more or less important energy levels and across different operability frequency ranges. However, although some of the rotary harvesters can be more compact and have higher energy density than the linear ones [**1**], their structure is usually more complex.

This is obvious for the following systems: the mechanical based transmission as ball screw mechanism [**4**], the simple [**5**- **6**] or double [**7**] rack-pinion mechanism, the hydraulic regenerative shock absorber [**8**-**10**] and the electromagnetic rotary damper [**11**] respectively. This complexity leads to a rise of both costs and structure modifications of the shock absorber or the automotive suspension.

Furthermore, the linear electromagnetic solution [**12**-**17**] and the spring mass system one [**18**] are the easiest to integrate comparing with other techniques such as the no-electromagnetic rotary type [**11**] and the linear type hydraulic system [**19**, **20**]. Among these solutions, the most accomplished ones is the electromagnetic linear system [**17**] which has been already successfully tested on the laboratory environment or road. Since the surface of magnetic circuit and the number of coils are optimized for the entire distance of the energy harvester movement, it allows output power at low speed. Consequently, this solution becomes increasingly attractive because of its high energy conversion efficiency, design simplicity, fast response, strong controllability and efficient capability in the energy recovery. Nevertheless, the main drawback of the current linear energy harvesters is still their size since this kind of structure provides at this time no place for the hydraulic part of a classic vehicle shock absorber.

B. Lafarge is with Université de technologie de Compiègne, Laboratoire ROBERVAL - FRE UTC - CNRS 2012 (e-mail: barbara.lafarge@uct.fr).

S. Grondel and C. Delebarre are with Univ. Polytechnique Hauts-de-France, CNRS, Univ. Lille, ISEN, Centrale Lille, UMR 8520 - IEMN - Institut d'Électronique de Microélectronique et de Nanotechnologie, DOAE - Département d'Opto-Acousto-Électronique, F-59313 Valenciennes, France (sebastien.grondel@uphf.fr and christophe.delebarre@uphf.fr).

O. Curea is with ESTIA Recherche, 64210 Bidart, France (e-mail: o.curea@estia.fr).

C. Richard is with LGEF Laboratory, INSA, University of Lyon, France (e-mail: claude.richard@insa-lyon.fr).

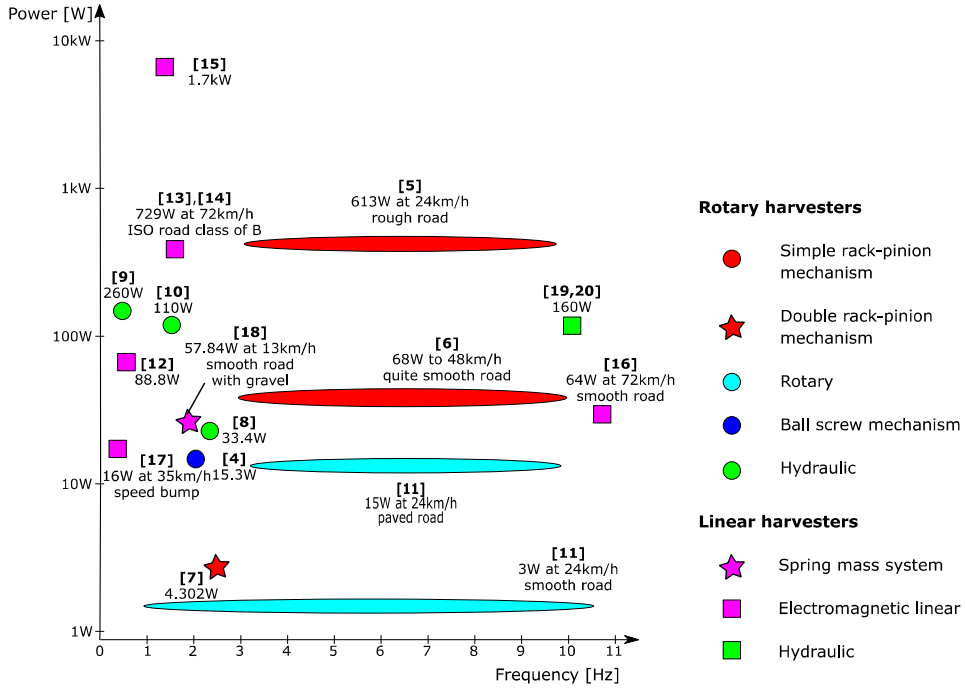

Fig. 1. Performances of energy harvester system embedded in a car suspension

In response to this problem, the authors have decided in this paper to design a new linear electromagnetic energy harvester directly embedded on a real shock absorber. Such a development requires solving many technological and scientific key issues. The first one deals with the choice of used materials to obtain an optimal energy conversion without changing the overall original structure of the suspension. A second one is a compromise to find between a maximum power harvesting while reducing at the same time as much as possible the magnetic force fluctuations due to the tooth of the magnetic circuit. The last challenge concerns the precise characterization of the non-linear electromagnetic coupling coefficient which is essential for the energy conversion.

In the **section II**, this paper presents the proposed design for the linear electromagnetic energy harvester embedded in the vehicle suspension. This system is composed of several subsystems: the car suspension, the linear electromagnetic energy harvester and the restitution electronic circuit. Taking care about the design, the analysis of the main parameters is done in the **section III**. In particular, the electronic, mechanical and electromechanical parameters are determined using a Finite Element analysis. In **section IV**, a Bond Graph (BG) model is developed to simulate the dynamic and power efficiency of the linear electromagnetic harvester. Simulations are then compared with the experimental results measured on a prototype.

III. SYSTEM DESCRIPTION

A. *Technical description*

The instrumented suspension can be divided into several subsystems (see **Fig. 2**): the first subsystem corresponds to the suspension itself, the second one to the electromagnetic harvester and the last one to the electrical circuit for managing and storage of the electrical energy. In this study, the energy harvester is embedded between the vehicle body (sprung mass) and the wheel (unsprung mass). This choice is motivated by the fact that the upper part of the rod outside the damper near the coil spring, despite a reduced space, is a region of high potential energy. The mechanical stresses applied to the suspension system are the input movements induced by the road profile.

In order to facilitate the integration of the harvester without disturbing the other mechanical elements, the permanent magnets are placed inside the rod and the coils in the shock absorber body. In addition, the orientation of the magnets is such that adjacent magnets oppose each other to act as magnetic flux guides around the coils. Finally, a magnetic circuit surrounding the coils is designed to optimize the passage of this magnetic field. This magnetic circuit is usually made of ferromagnetic material through which the magnetic induction flux flows (see **Fig. 4**).

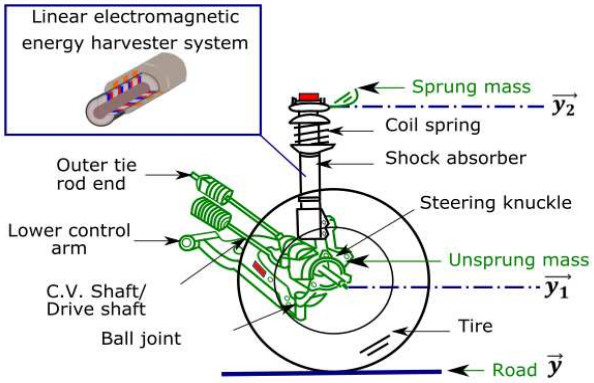

Fig. 2. Suspension system with the energy harvester embedded on the shock absorber

B. Theoretical study

The linear electromagnetic energy harvester can be divided also into two subsystems (**Fig. 3-a**). The first one describes the transformation of the mechanical energy into electrical energy, whereas the second one corresponds to the electrical circuit coupled to this conversion for the electrical energy recovery. In this case, the voltage at the outputs of the electromagnetic element and of the load circuit are equal to $V(t)$.

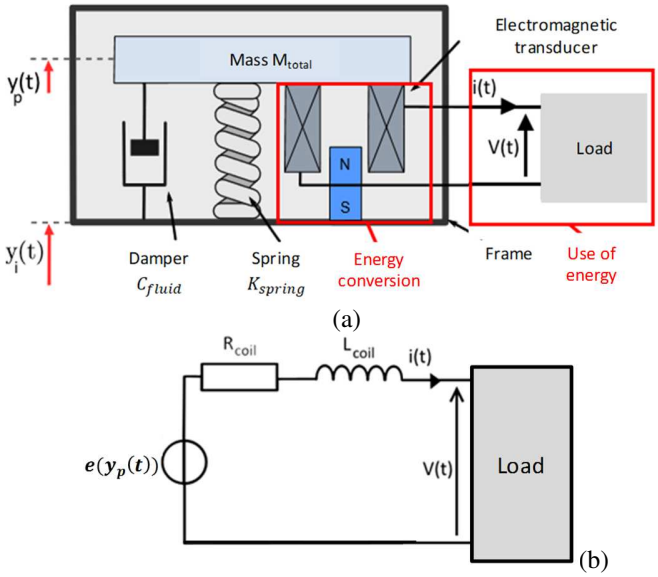

Fig. 3. (a) Energy extraction circuit [**21**] and (b) equivalent electrical circuit representing the linear electromagnetic harvester [**21**]

In order to take into account the energy source characteristics, it is also necessary to add a mass-spring-damper type representation in parallel with the mechanical energy conversion subsystem (**Fig. 3-a**). This part which mechanically includes the energy transformation, symbolizes the physical structure in which the active components, i.e. the electromagnetic harvester and the magnet are located. It is represented using damping C_{fluid} of the shock absorber, inertia M_{total} and stiffness K_{spring} elements. Here the mass M_{total} is shared between the sprung mass and the unsprung mass of the suspension. When a mechanical stress is applied to the shock absorber, this results in the displacement $y_p(t)$ of the electromagnetic harvester with respect to the magnet. $y_i(t)$ here corresponds to the displacement imposed on the shock absorber.

If we focus on the electromagnetic harvester, it can be modeled using the equivalent electrical circuit shown in **Fig. 3- b**. It consists of a voltage source $e\left(y_p(t)\right)$ proportional to the translation velocity $\dot{y}_p(t)$ and an electromagnetic coefficient depending on this translation, in series with the inductance of the coil L_{coil} and its resistance R_{coil}. Therefore, we assume as the electromotive force (e) and the position (y_p) is a composion of function e and y_p expressed as $(eoy_p)(t) = e\left(y_p(t)\right)$. Using the equivalent circuits, we can easily deduce both a mechanical equation (1.a) and an electrical one (1.b) [**22**]:

$$\begin{cases} M_{total}\dfrac{d^2y_i(t)}{dt^2} = M_{total}\dfrac{d^2y_p(t)}{dt^2} + C_{fluid}\dfrac{dy_p(t)}{dt} + \cdots & \\ K_{spring}y_p(t) + r\left(y_p(t)\right)i(t) & (1.a) \\ e\left(y_p(t)\right) = (R_{coil} + R_{load})i(t) + L_{coil}\dfrac{di(t)}{dt} & (1.b)\ (1.c) \\ e\left(y_p(t)\right) = r\left(y_p(t)\right)\dfrac{dy_p}{dt} & (1.d) \\ F_{mag}\left(y_p(t)\right) = r\left(y_p(t)\right)i(t) & \end{cases}$$

where R_{load} corresponds to the load resistance.

The movement $y_p(t) = y_2(t) - y_1(t)$ of the sprung mass $y_2(t)$ relativity to the unsprung mass $y_1(t)$ induces a translation of the shock absorber body containing the coils with respect to the stack of permanent magnets located in the rod as shown in **Fig. 10**. This results in a current in the coils $i(t)$ and therefore a voltage $V(t)$ measurable at the linear electromagnetic harvester output. At the end, the electric energy can be stored or directly used to simulate the function of a real electrical load.

Nevertheless, it should be noted that this system presents a non-linear effect because the magnetic force $F_{mag}\left(y_p(t)\right)$(1.d) belonging to the mechanical equation (1.a) and the electromotive force $e\left(y_p(t)\right)$ (1.c) of the electrical equation are both functions of a non-linear term $r\left(y_p(t)\right)$ which depends on the position $y_p(t)$. $r\left(y_p(t)\right)$ is the mechanical-electrical coupling term. A key issue for the design of the electromagnetic harvester is to be able to characterize these functions, therefore it is essential to describe more precisely the structure of the electromagnetic harvester.

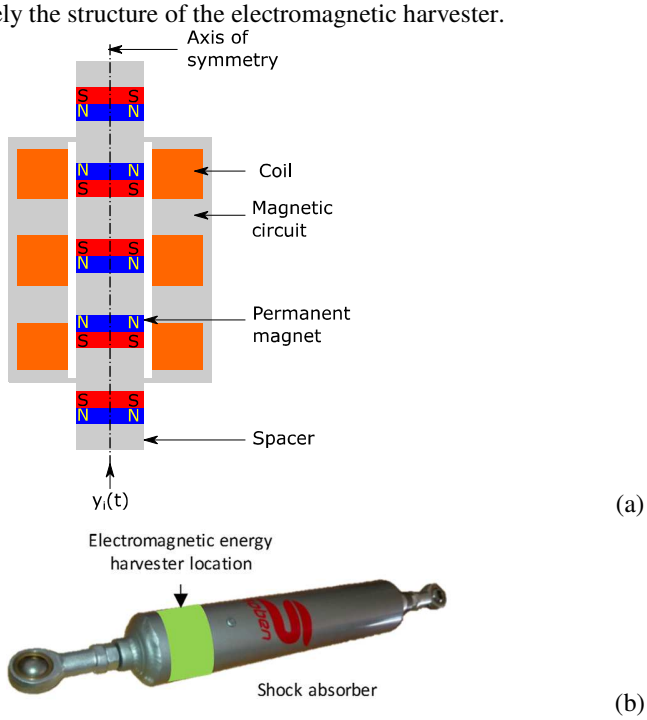

Fig. 4. Cross sectional view of the electromagnetic energy harvester (a) and the prototype embedded in the shock absorber (b)

As shown in **Fig. 4-a**, the electromagnetic structure is axisymmetric. Compared to the structure shown in **Fig. 3-a**, **Fig. 4-a** takes into account several layers of coils and magnets [**23**] to increase the energy performance of the system. Let us now present the relevant equations arising from such a system. According to Lenz-Faraday's law [**24**], the electromotive force depends on the distribution of the magnetic induction flux ϕ circulating in the coil:

$$e\left(y_p(t)\right) = -N_{coil}\frac{d\phi\left(y_p(t)\right)}{dt} \tag{2}$$

with N_{coil} the number of the turns contained in a coil.

It is clear from the literature that this calculation of magnetic induction fluxes strongly depends on the chosen configuration and is fundamentally non-linear. Some authors have recently worked to solve analytically this problem [**23**] and [**25**-**28**]. Nevertheless, the disadvantage is that it requires to determine experimentally all the parameters, which is not always possible.

In our case, we propose another approach. As a main assumption, we consider that the magnetic induction flux seen by each turn is the same and is described by equation (3):

$$\phi\left(y_p(t)\right) = \int_{\substack{coil \\ section}} B(y_p(t))dS \tag{3}$$

Since the distribution of the magnetic induction B as function of the space and time for the chosen configuration remains very complex, its computation is obtained using the finite element method (see **section III**).

Note that the index i indicates the number of considered coils (we consider three coils). We obtain the following expression (4):

$$e_i\left(y_p(t)\right) = -N_{coil\_i}\frac{d\phi_i\left(y_p(t)\right)}{dt} \tag{4}$$

In order to express equation (4) as a function of the mechanical-electrical coupling term $r\left(y_p(t)\right)$, we can rewrite this expression as follows, with the derivative of the composite function:

$$e_i\left(y_p(t)\right) = -N_{coil\_i}\frac{d\phi_i\left(y_p(t)\right)}{dy_p}\frac{dy_p}{dt} \tag{5}$$

Thus, we obtain:

$$e_i\left(y_p(t)\right) = r_i\left(y_p(t)\right)\frac{dy_p}{dt} \tag{6}$$

Knowing that each coil is characterized by an inductance L_{coil_i} and a resistance R_{coil_i}, it is possible to deduce the expression of the output voltage $V(t)$ of each coils using the Kirchhoff laws [**29**] for coils connected in parallel, as shown in **Fig. 5-a**.

$$V(t) = -L_{coil\_i}\frac{di_i(t)}{dt} - R_{coil\_i}i_i(t) + e_i\left(y_p(t)\right) \tag{7}$$

The coils can be connected to the external electrical circuit in two ways, either in series or in parallel. A series connection gives a high output voltage with a low current across a load, while conversely, a parallel connection induces a low voltage with a higher output current. Consequently, the power is identical for these two configurations and only the voltage/current proportions vary. In our case study, the authors have chosen the parallel configuration as shown in **Fig. 5-a** to obtain a high current with respect to the voltage. The power recovered across a resistance R_{load} for coils in parallel is as followed:

$$P(t) = R_{load}i(t)^2 \tag{8}$$

with $i(t)$ the sum of current crossed the coils.

$$i(t) = \sum_{i=1}^{3} i_i(t) \tag{9}$$

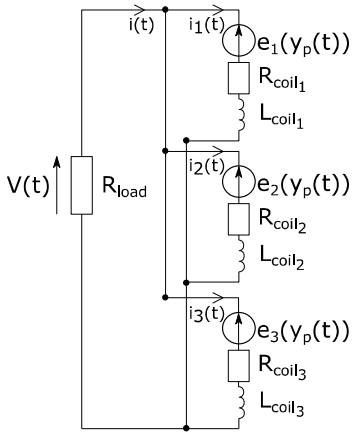

(a)

LEH: linear electromagnetic energy harvester

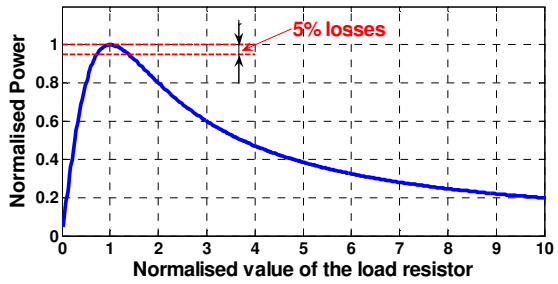

(b)

Fig. 5. (a) Electrical circuit representative of the coils in parallel connection connected with a resistive load R_{load}, and (b) the variation of output power according to load resistor value

Fig. 5-b illustrates the normalized power variation (output power divided by its maximum) with regard to the normalized value of the load resistor (value of the load resistor divided by the equivalent resistance of the coils). The output power is maximized by a load resistor that matches the value of the equivalent resistance of the coils. In this case, the same power will be dissipated on the coil and load resistance and it is obvious that electrical efficiency cannot exceed 50%. For a different resistor, the output power decreases. If the value of the resistor is lower, the current increases, but more power will be dissipated on the coils and if the value is higher, the output current decreases and the power lost on the coils will be lower. However, output power losses do not exceed 5% for a variation of the normalized resistance from 0.73 to 1.38.

To obtain experimentally the maximum power, the technical solution are to measure directly the current and voltage across the load resistance or for more precision to use a Maximum Power Point Tracking (MPPT) algorithm with its associated converter. The last technique is used commonly to maximize power extraction under all conditions [**30**].

With the help of the fundamental principle of dynamics which describes the relative movement of magnets with respect to coils caused by the excitation imposed by the road through the unsprung mass [**28**, **31**], it is possible to achieve the expression below:

$$m_{sm}\frac{d^2y_2(t)}{dt^2} = m_{sm}\frac{d^2(y_2(t)-y_1(t))}{dt^2} + C_{fluid}\frac{d(y_2(t)-y_1(t))}{dt} + K_{spring}\left(y_2(t)-y_1(t)\right) + F_{mag_{total}}\left(y_p(t)\right) \tag{10}$$

It remains then to determine the magnetic force for each coil $F_{mag_i}\left(y_p(t)\right)$ corresponding to the term $r_i\left(y_p(t)\right)i_i(t)$. It is obtained from a power balance on the electromagnetic system such as:

$$F_{mag_i}(y_p(t))\frac{dy_p(t)}{dt} = e_i(y_p(t))i_i(t) \tag{11}$$

It is then possible to replace the electromotive force by its expression given in equation (2) and thus by coil, one obtains:

$$F_{mag_i}(y_p(t))\frac{dy_p(t)}{dt} = -N_{coil\_i}\frac{d\phi_i\left(y_p(t)\right)}{dt}i_i(t) \tag{12}$$

By generalizing the equation (12) for all the coils and taken into account the generated force by the external tooth noted $F_{ext_{\text{tooth}}}\left(y_p(t)\right)$ we can deduce that:

$$\left(F_{mag_1}\left(y_p(t)\right) + F_{mag_2}\left(y_p(t)\right) + F_{mag_3}\left(y_p(t)\right) + F_{ext_{\text{tooth}}}\left(y_p(t)\right)\right)\frac{dy_p(t)}{dt} = -\left(N_{coil_1}\frac{d\phi_1(y_p(t))}{dt}i_1(t) + N_{coil_2}\frac{d\phi_2(y_p(t))}{dt}i_2(t) + N_{coil_3}\frac{d\phi_3(y_p(t))}{dt}i_3(t) - F_{ext_{\text{tooth}}}\left(y_p(t)\right)\right) \tag{13}$$

Note that we have added the complementary term corresponding to the tooth which will be measured at very slow speed. This term can then be rewritten as follows:

$$F_{mag_1}\left(y_p(t)\right) + F_{mag_2}\left(y_p(t)\right) + F_{mag_3}\left(y_p(t)\right) + F_{ext_{\text{tooth}}}\left(y_p(t)\right) = -\left(N_{coil_1}\frac{d\phi_1(y_p(t))}{dy_p}i_1(t) + N_{coil_2}\frac{d\phi_2(y_p(t))}{dy_p}i_2(t) + N_{coil_3}\frac{d\phi_3(y_p(t))}{dy_p}i_3(t) - F_{ext_{\text{tooth}}}\left(y_p(t)\right)\right) \tag{14}$$

Hence the total magnetic force $F_{mag_{totale}}(y_p, t)$ can be deduced from the following relationship:

$$F_{mag_{total}}(t) = r_1\left(y_p(t)\right) i_1(t) + r_2\left(y_p(t)\right) i_2(t) + r_3\left(y_p(t)\right) i_3(t) + F_{ext_{\text{tooth}}}\left(y_p(t)\right) \quad (15)$$

The key issue hereafter is to maximize the harvester power at the output of the electromagnetic harvester without degrading the dynamic shock absorber behavior. A compromise on both the geometry and the location of the electromagnetic harvester has to be found in order to increase the energy conversion.

Using equation (4), a flux optimization of the magnetic induction can be obtained by adjusting both the geometry, i.e. the size of the coils and the configuration of the magnetic circuit. Furthermore, the electromagnetic coupling term, seen in expressions (6) and (15), is a non-linear one and requires a thorough characterization. Another key issue is the electromagnetic harvester location which plays a main role in energy recovery. Indeed, the higher the displacement speed applied to the harvester is, the greater the obtained energy levels are as shown in equation (1). Notice that the maximum energy level remains however limited because of the material magnetic saturation and the actually available space inside the rod. Consequently, the harvester mechanical structure as well as its electrical part would have to be adapted to the characteristics of the energy source.

IV. PARAMETERS ANALYSIS

A. *Parameter's definition*

When designing the electromagnetic energy harvester, a first key issue is that its integration does not interfere with the car damper linear movement whereas a second key issue is that it also not brings major changes in the suspension laws. We will see in the **section III-B** that the tooth forces have a negative impact on it, so the design aim will be to reduce the circuit magnetic's dentition phenomena to +/- 20N. This value is acceptable because it is less than 10% of the shock absorber's damping force and may be decreased in future works. To achieve this range of strength, several techniques can be proposed: either one can modify the magnetic circuit and the elements location of the electromagnetic harvester or move the magnets away from the magnetic circuit.

TABLE I
MATERIAL AND ELECTROMAGNETIC PARAMETERS OF THE TESTED ENERGY RECOVERY SYSTEM

Parameters		Values	Unity
R_{coil_1}	Coil's resistance n°1	145.6	Ω
n_{coil_1}	Number of turns of the coil n°1	1820	N/A
R_{coil_2}	Coil's resistance n°2	144.9	Ω
n_{coil_2}	Number of turns of the coil n°2	1806	N/A
R_{coil_3}	Coil's resistance n°3	148.1	Ω
n_{coil_3}	Number of turns of the coil n°3	1840	N/A
R_{load}	External load resistance	46.5	Ω
$L_{coil_{1,2\,ou\,3}}$	Coil's inductance n°1, 2 or 3	104.4	mH

The chosen solution (**Fig. 4-b**) is to adapt the elements location of the electromagnetic harvester and to redraw the magnetic circuit surrounding the coils as shown in **Fig. 4-a** and **Fig. 6**. The designed damper is therefore much easily inserted into the actual suspension system of the vehicle. The key parameters are summarized in **Table I**.

B. *Finite Element Method (FEM) simulation*

To determine the magnetic forces generated by each of the three coils as well as by the tooth of the magnetic circuit, such as the external cages whose position is given in **Fig. 6**, it is first necessary to analyze the derivative of the flux evolution of magnetic induction computed with a static FEM analysis (see **Fig. 7-a**).

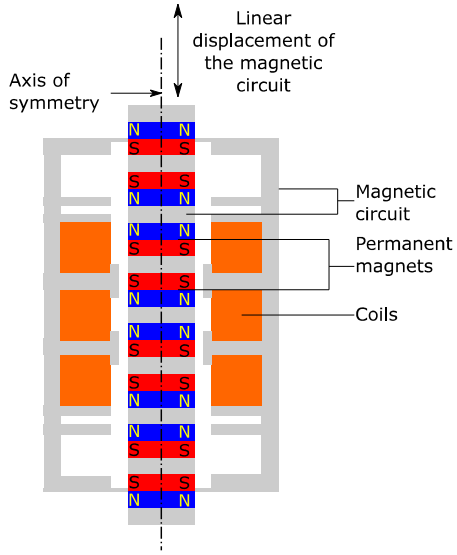

Fig. 6. New magnetic circuit topology integrated into a shock absorber considering the magnetic forces reduction

More precisely, this first step leads us to characterize the nonlinear coefficients $r_1\left(y_p(t)\right)$, $r_2\left(y_p(t)\right)$ and $r_3\left(y_p(t)\right)$ corresponding to the magnetic circuit portions surrounding the coils (**Fig. 7-b**) since they are directly dependent on the derivation calculation of the magnetic induction flux as underlined in the expression (4). Notice that their value summarized in **Table II** as example for a given velocity can be used as an input variable in the BG model as shown in **section IV**.

TABLE II
PARAMETERS INTEGRATED IN THE BOND GRAPH MODEL FOR $V = 0.75m/s$ AND $R_{load} = 46.5\Omega$

Parameters	Amplitude	Unity	Frequency	Unity
$r_i\left(y_p(t)\right)$ Coupling terms for $i = 1\ to\ 3$	[-22, 22]	N/A	11.21	Hz
$F_{ext_{\text{tooth}}}\left(y_p(t)\right)$ Force generated by the external tooth	[20 74]	N	10.86	Hz

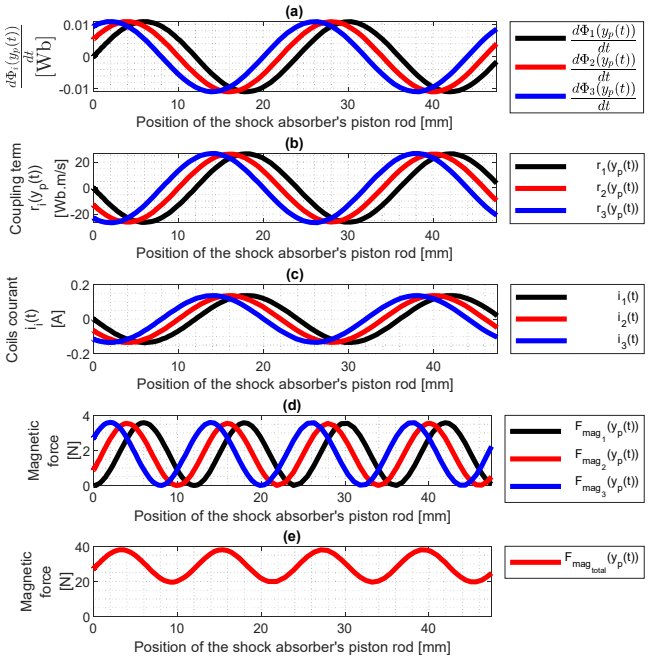

Fig. 7. (a) FEM Magnetic induction flux seen by each of the coils and in the so-called "upper zone" (see the **Fig. 6**), (b) computation of the non-linear term $r_i(y_p(t))$ for each of the coils and (c) current evolution, (d) simulated magnetic forces for each coil and (e) resulting total magnetic force

It is supposed in this case that the magnetic fields induced by the coil current are small compared to the magnet coercive field so that they do not modify significantly the global magnetic flux.

In a second step, the generated magnetic forces (**Fig. 7-d**) are deduced from the currents present in the coils (**Fig 7-c**) as shown in equation (12). Finally, the total magnetic force (**Fig. 7-e**) is the sum of these generated magnetic forces and the tooth force of the magnetic circuit.

C. Comparison between simulations and test results in a static mode

The tests carried out on the prototype are intended to understand the involved phenomena on the one hand and to validate the static finite element simulations on the other hand. It is question of being able to quantify the value of magnet attraction forces/magnetic circuit without any coil as well as to observe the different parameters influence [**23**, **28**] on its intensity.

As shown on **Fig. 8**, this part is the first phase of the study of finding the right location for the magnetic circuit. The prototype tested in this section is a simplified version of the energy harvester, since only the magnets, the spacers and the magnetic circuit surrounding the coils are present. The coils are not present. More precisely, the prototype consists of a part of the magnetic circuit which corresponds to a simple disc in translation with the rod containing magnets separated by spacers (see **Fig. 8- a**) without coil. This configuration was specially developed in order to minimize the effects of frictional forces due to fluids, sealing elements, such as lip seals and O-rings, and the mechanical friction between elements, as well as the electromotive force. Therefore, frictions between the elements of the electromagnetic harvester are reduced at their minimum in order to measure only the magnetic forces induced by the magnetic circuit structuring, i.e. the tooth effect.

In practice, this means that the shock absorber prototype including a simplified circuit magnetic (**Fig. 8-a** and **8-c**) is installed on a hydraulic test bench shown in **Fig. 8-b**. Furthermore, only the lower part of the shock absorber is set in motion which corresponds to $y_p(t)$ while the upper part remains static.

Then, a BC302 strain gauge used as force sensor is fixed on the shock absorber (**Fig. 8-a**) to deduce with a better precision than the S-beam load cell the forces acting on the system. In this configuration, the weight of the discs has no effect on the measurement system. The force sensor has been calibrated to cancel the weight of the rod. Moreover, the conventional interface of the test bench has been modified (**Fig. 8-b**) to vary the position of the rod containing the magnets with respect to the teeth, millimeter by millimeter at a very low speed of 0.001m/s. The speed is as low as possible. We assume a quasi-static movement. In this measurement, there is no current. This approach allows the measurement of the magnetic instantaneous force.

The magnets and the steel parts in the rod and intercalated between them have a height of 8mm and 4mm respectively, while the thickness of the disc representing part of the magnetic circuit leading the flux lines is equal to 3mm. Note that the middle position of the magnetic circuit is indicated on the upper part of **Fig. 9.**

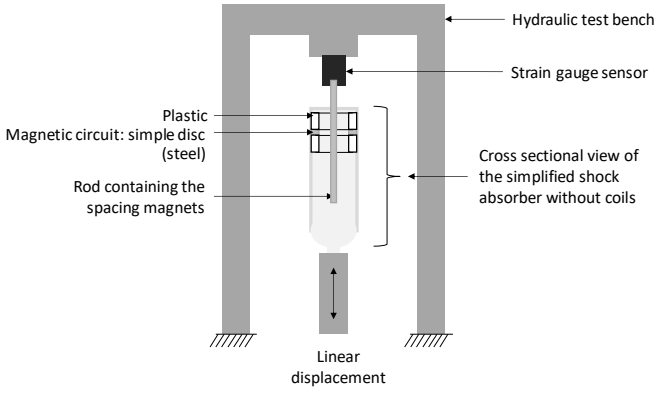

(a)

(b)

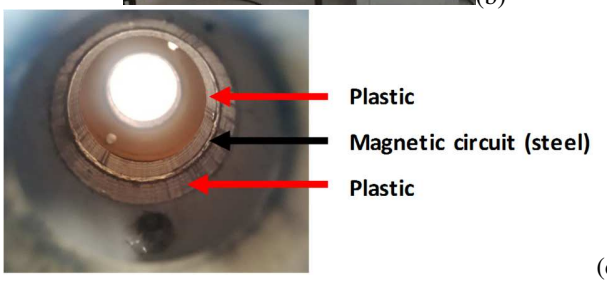

(c)

Fig. 8. Equipment for tests (a) and (b): the hydraulic test bench, cross view of the shock absorber (c) and the strain gauge sensor

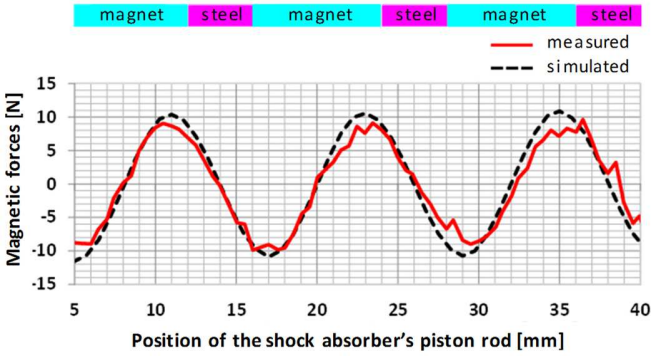

Fig. 9. Experimental and FEM results

After analysis of the results, it can be observed that the measured magnetic forces vary mostly sinusoidally with an amplitude of +/-10N for a single disc (**Fig. 9**). However, it is necessary to have two discs of the same thickness to properly conduct magnetic field lines around a coil. As expected, the additional disc increases considerably the magnetic forces. The obtained result confirms that the magnetic induction flux varies sinusoidally as a function of its position in the magnetic circuit.

The experimental results obtained are then compared to the FEM simulation ones. As expected, the comparison is in good keeping. Indeed, the difference between the results is less than 6.75% (**Table III**) which validates the simulation.

TABLE III
DIFFERENCES BETWEEN THE MEASUREMENTS AND THE SIMULATIONS

Speed [m/s]	Magnetic force measured on a disc [N]		Gap [%]
	Simulated FEM	Experience	
0.001m/s	10.08N	9.4N	6.75%

It should be also noticed that various topological configurations of the magnetic circuit have been also tested which demonstrated that it was possible to increase or decrease this magnetic force just by changing the position and adding steel discs.

V. DYNAMIC EFFICIENCY OF THE ELECTROMAGNETIC ENERGY HARVESTER

A. Bond Graph model of the electromagnetic energy harvester embedded on the shock absorber

In order to analyze the dynamic efficiency of the electromagnetic harvester, the BG method is proposed since it allows taking into account both the mechanical behavior of the suspension as well as the electromagnetic harvesting and at the same time characterizing the power exchanges inside the system.

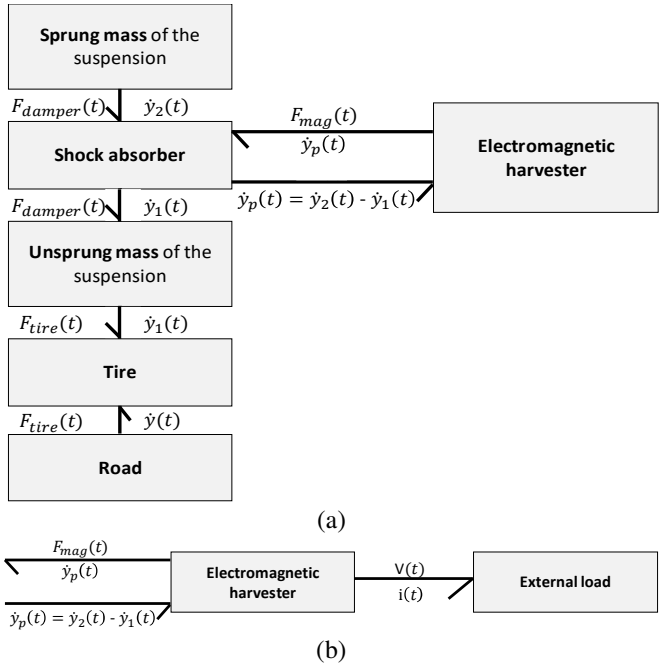

Fig. 11. Word Bond Graph of the suspension system with the electromagnetic harvester embedded on the shock absorber

The first step is therefore to establish the word BG of the global system (see **Fig. 10**). This word BG is deduced from **Fig. 2** and represents the suspension system divided into subsystems helping to have a general overview of the topic. The input and output of each subsystem define power variables represented by a half arrow. Variables used for this studied system are the mechanical variables $(Force, Linear\ velocity) = (F, \dot{y})$ and the electrical ones $(Voltage, Current) = (V, i)$.

The second step lies in finding the BG model of each subsystem. As the BG subsystems of the road suspension system as well as the power storage and restitution circuit have been lengthy developed in [**2**], only the electromagnetic harvester subsystem will be detailed here. To determine its BG model, the equations (6), (7) and (14) of the electromagnetic conversion system are used. In this case, the BG dissipative element R and the BG storage element I represent the resistance R_{coil_i} and the inductance L_{coil_i} of each coil respectively.

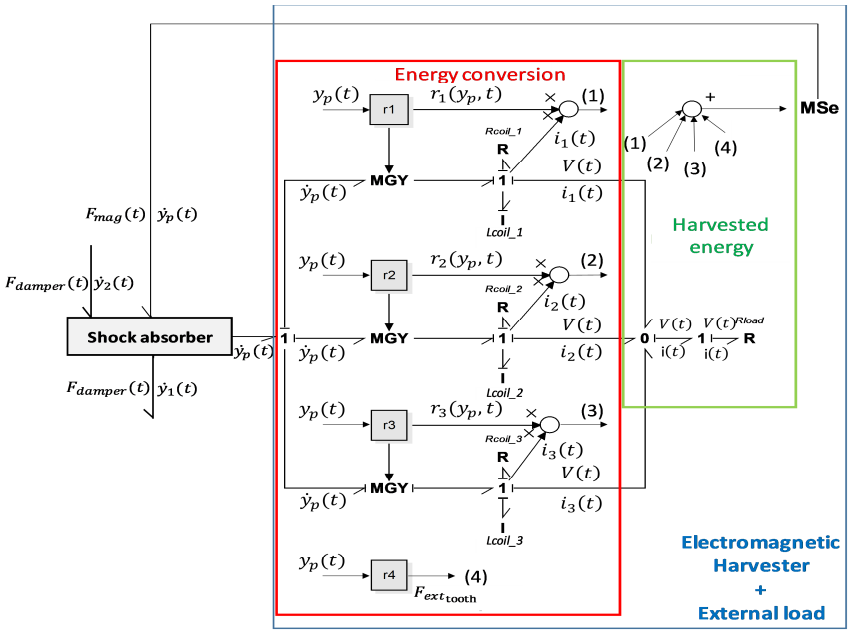

Fig. 11. Bond Graph model of the electromagnetic harvester

LEH: linear electromagnetic energy harvester

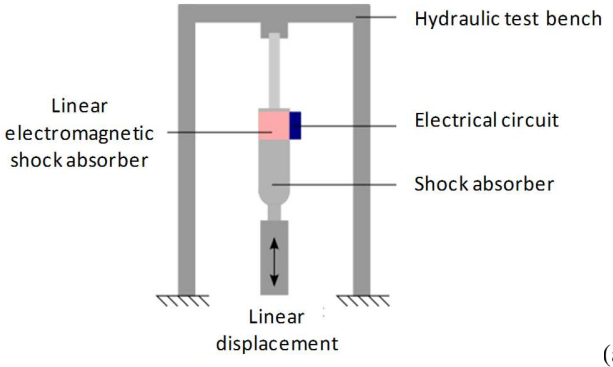

(a)

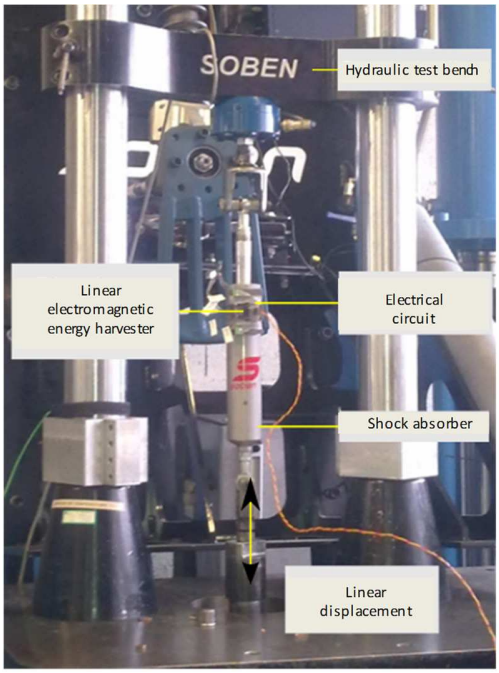

(b)

Fig. 12. Electromagnetic harvester prototype embedded on a shock absorber and mounted on a hydraulic test bench

The power exchange between the electrical and mechanical subsystems of each coil is represented by the modulated gyrator MGY whose modulation ratio corresponds to the non-linear function $r_i(y_p(t))$. The index i indicates the highlighted coil. The 0 junction results directly from the Kirchhoff's current law whereas the 1 junction reflects the Kirchhoff's voltage law in each coil. Note that the generated force by external tooth $F_{ext_{\text{tooth}}}(y_p(t))$ is evaluated from experiments, and is required for the computation of the global magnetic force. The resulting BG model of this subsystem is shown in the **Fig. 11**.

B. Energy harvesting validation in a laboratory environment

In order to demonstrate the validity of the approach in a real case, the electromagnetic shock absorber prototype (**Fig. 4-b**) is mounted on a hydraulic bench (**Fig. 12**). Note that the movement of the hydraulic bench does not exceed 49mm and is imposed through a linear velocity. Contrarily to previous experiments, the tests are carried out in dynamics. **Fig. 13** presents the curves of the voltage and the power measured and simulated on the same optimal load ($R_{load} = 46.5\Omega$) for two different velocities: 0.75m/s and 1m/s respectively.

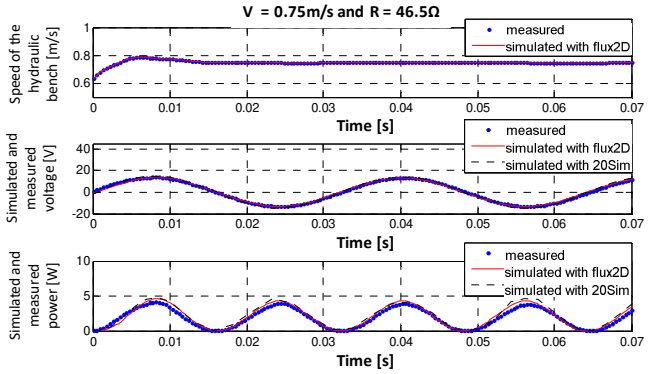

(a)

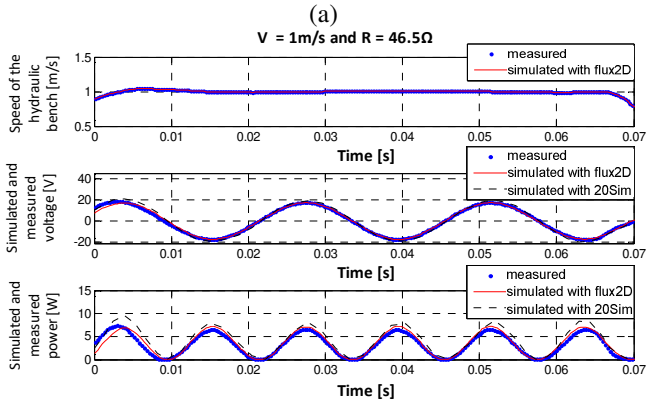

(b)

Fig. 13. Instantaneous power and voltage curves for a load resistance value of 46.5Ω and a linear velocity of (a) 0.75m/s, (b) 1m/s

As expected, the results of the simulation and experiments are in good correlation, since the interval error between the measured and simulated results is less than 6% (**Table IV**). The obtained maximum amplitudes of the voltages and the power are equal to 15V and 4W for a solicitation of 0.75m/s respectively while they reach 20V and 7W for a solicitation of 1m/s. Another significant result is the sinusoidal variation of the voltages and powers curves which validates our initial assumption that the flux inside the coils varies sinusoidally.

Figure 14 represents the variation of the magnetic forces for two different velocities. When the velocity is equal to 0.75m/s, the variation of the magnetic forces is approximately 18N (**Fig. 14-a**) while it increases slightly for a velocity of 1m/s (**Fig. 14-b**). This variation of the magnetic force is added to the friction forces present in the shock absorber.

The **Table V** summarizes all the results. The observed maximum differences between the experiments and the FEM and BG simulations methods are equal to 26.2% and 33.3% respectively. As showed by [**23**], it could be possible to develop more precise computations but this will undoubtedly require to develop an experimental device to accurately estimate the magnetic induction flux variation. Although, this difference stays important, it allows however to quantitatively estimate generally the magnetic force generated by the magnetic circuit.

Furthermore, all these results are physically coherent as demonstrated below. Let us consider first the measured energy (16) for a complete cycle:

$$E = \int_{full\ cycle} Fdx = 2 \times F_{mean} \times \Delta x \tag{16}$$

at $V = 0.75\mathrm{m/s}$ and $V = 1\mathrm{m/s}$ which is equal to 2.17J and 2.64J respectively and second the cycle time (17):

$$\Delta t = \frac{2 * \Delta x}{V} \tag{17}$$

equal to 0.1261s and 0.0945s for 0.75m/s and 1m/s respectively, then the combination of these expressions leads to the generated power (18).

$$P = \frac{\int_{full\ cycle} F dx}{\Delta t} \tag{18}$$

The maximum power for a complete cycle is then equal to 17.25W and 28W for 0.75m/s and 1m/s respectively, a part of this energy is converted in electrical energy, which is consistent with the results of **Table IV**. Note that F represents the integral of the magnetic force i.e. 23N at 0.75m/s (**Fig. 14-a**) and 28N at 1m/s (**Fig. 14-b**) whereas $\Delta x = 47.27mm$ is the travel distance for a half cycle.

These first results are encouraging since the energy available at the output of the proposed electromagnetic energy harvester of the order of 10 Watts appears sufficient to power a classical electronic circuit. Moreover, magnetic forces remain important but have been largely reduced.

TABLE IV
RESULTS OF SIMULATIONS AND EXPERIENCES FOR DIFFERENT IMPOSED VELOCITIES

Velocity [m/s]	Maximal peak voltage [V] from prototype					Maximal peak power [W] from prototype				
	FEM n°4	BG	experiment	gap FEM/exp [%]	gap BG/ exp [%]	FEM n°4	BG	experiment	gap FEM/exp [%]	gap BG/ exp [%]
0.75m/s	15.15V	15.1V	15V	1%	0.66%	4.21W	4.2W	4W	5.25%	5%
1m/s	20.1V	19.9V	20V	0.5%	1.5%	7.2W	7.15W	7W	2.85%	2.14%

TABLE V
RESULTS OF SIMULATIONS (FEM AND BG) AND EXPERIENCE FOR DIFFERENT SPEEDS IMPOSED AT THE INPUT OF THE MODEL

Velocity [m/s]	Magnetic force [N] from prototype				
	FEM n°4	BG	experiment	gap FEM/exp [%]	gap BG/exp [%]
0.75m/s	31N	28N	42N	26.2%	33.3%
1m/s	38N	34N	50N	24%	32%

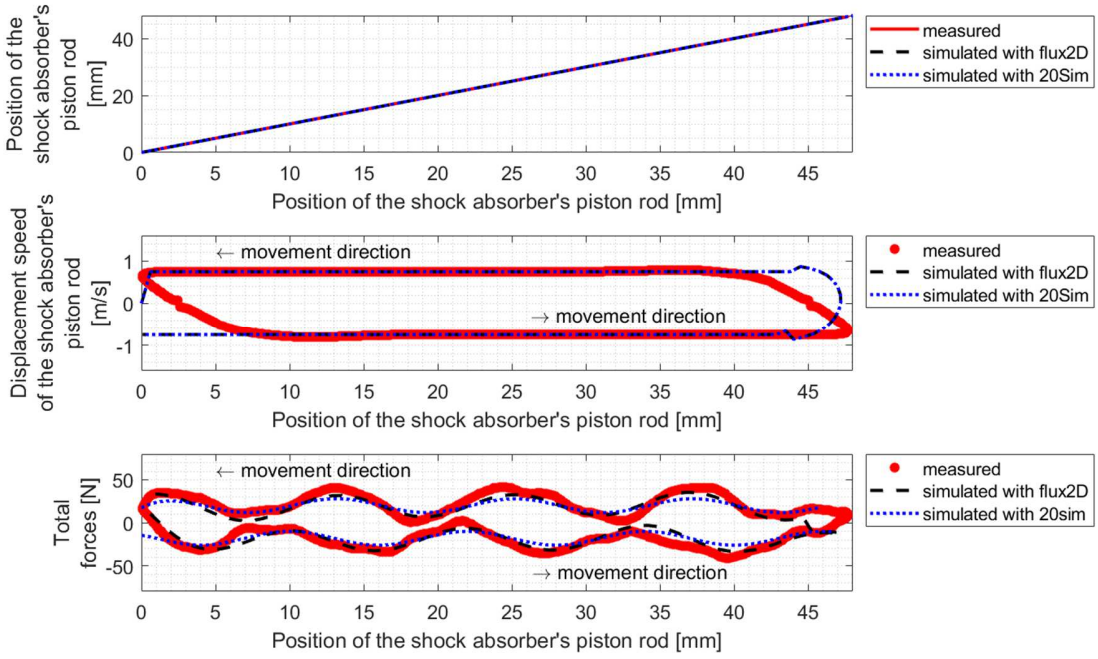

(a)

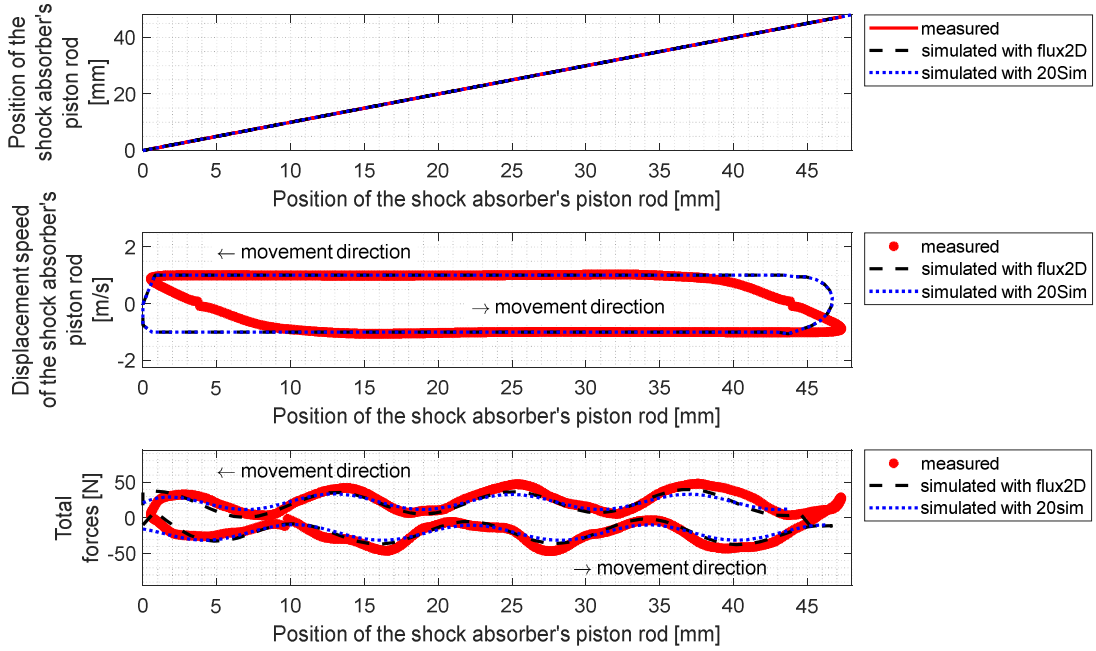

(b)

FIG. 14. TOTAL FORCES MEASURED FOR A LINEAR SPEED OF (A) 0.75M/S (B) OF 1M/S

C. Simulation of the global model

In order to demonstrate the validity of the approach, simulation tests have been performed with the whole energy harvester system embedded in a vehicle model. Moreover, two different situations have been experimented: the first situation corresponds to drive through a speed bump at 30km/h, whereas the second one coincides with driving test at 20km/h on a road of A-B class and E-F class respectively.

Table VI summarizes all the mechanical parameters injected on the vehicle system. The analysis of the simulated harvester power signals demonstrated that the energy is significant on a long period and could be used to supply sensors. **Fig. 15** illustrates the voltage and power simulated as function of the time measured through the optimal load resistance (R_{load}). The maximal output voltage range obtained is close to 22.26V with a maximal output power of 10.67W during the speed bump excitation. The average power value is 4.4mW.

TABLE VI
MECHANICAL PARAMETERS OF THE VEHICLE SYSTEM [**32**]

Symbol	Parameters	Values	Units
M_{sm}	Sprung mass	897.2	kg
K_{spring}	Suspension stiffness	66824.4	N/m
C_{fluid}	Suspension damping	1190	Ns/m
M_{usm}	Unsprung mass	87.15	kg
K_{tire}	Tire stiffness	101115	N/m

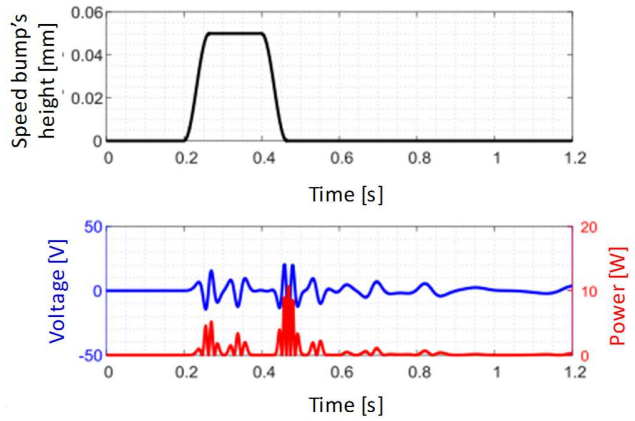

Fig. 15. Simulated voltages and powers with a load resistance value of 46.5Ω in case of driving through a speed bump with a car speed of 30km/h

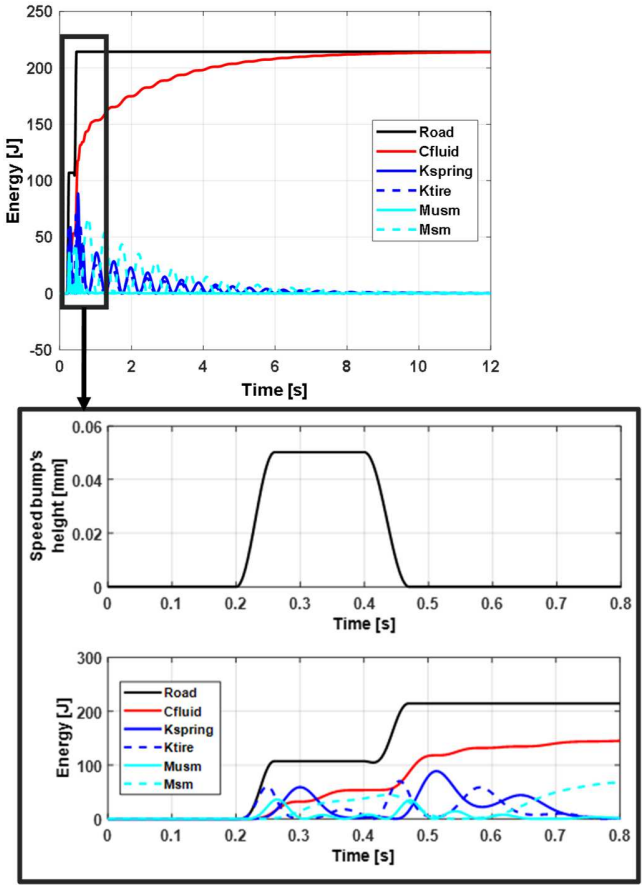

Fig. 16. Evolution of the total injected energy (in black), total kinetic energy (in cyan), total potential energy (in blue) and total dissipated energy (in red) for the suspension subsystem

To know the energy distribution in the global system, it is relevant to study its evolution in all the subsystems (**Fig. 16** and **17**). The simulated injected energy to the suspension parts by the road is 208J. The energy is then decomposed in three different ones. The main part is dissipated through friction in the car damper (C_{fluid}) and in the electromagnetic energy harvester (R_{coil} and R_{load}). In parallel, less quantity is stored in potential energy (K_{tire} and K_{spring}) and in kinetic energy (M_{usm} and M_{sm}). **Figure 16** illustrates the total energy, i.e. the injected, dissipated and stored (potential and kinetic) energy as function of the time, in the mechanical parts of the suspension. The obtained responses reflect the behavior of the dual-mass for the mechanical domain. Between 0.2s and 0.26s, the car goes up to the speed bump and goes down from 0.4s to 0.47s. After 0.47s, there is no variation of the road height. Indeed **Figure 16** shows that the K_{tire} stored energy increases first between 0.2s and 0.236s which means that the injected energy is stored in the first mechanical part closest to the road, then the K_{spring} stored energy in second time between 0.222s and 0.3s. The energy begins to dissipate in C_{fluid} at 0.225s. As the injected energy is stopped to increase at 0.24s and that all this energy is transferred to all mechanical elements, the stored and dissipated energy drop.

LEH: linear electromagnetic energy harvester

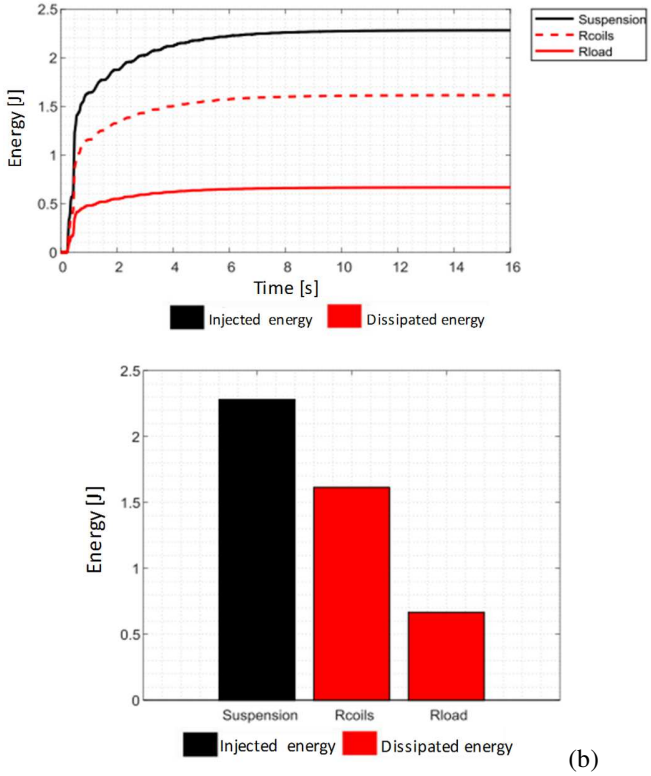

Fig. 17. Evolution of the injected energy by the electromagnetic system (in black) and total dissipated energy (in red) for the electromagnetic energy harvester subsystem

This behavior is reproduced when the car goes down. When the car goes down, the injected energy is constant and tends towards 207.6J. After a long time of 12s, the injected energy is totally dissipated in C_{fluid} and the system converges to a stable state. The kinetic energy (M_{usm} and M_{sm}) and the potential energy (K_{tire} and K_{spring}) cancel after several fluctuations due to the storage and then the restoration of energy.

It was also possible to simulate the injected and dissipated energy in the electromagnetic energy harvester (see **Fig. 17**). The injected energy is mainly dissipated both in the coils (R_{coil}) (i.e. 70.75% of the injected energy) and in the load (R_{load}) (29.24% of the injected energy). From these curves, it was also possible to determine the electromagnetic efficiency which is equal to $\eta = 0.2924$.

When the external load value coincides with the coils equivalent resistance, an optimal repartition of the energy in the system should be obtained and this repartition would correspond to 50% for all the coils and 50% in the load. However, the phase difference between the coils as shown in **Fig. 17** reduces considerably this repartition, which explains why we do not obtain such a result.

The analysis of the simulated harvester power signals with a generated artificial profile [**34**] based on the equation provided by ISO 8608 standard at 20km/h demonstrated that the harvested energy is significant on a long period and could be used to supply sensors. Indeed, from **Fig 18-a** and **19-a**, the maximal power value is in the order of 75mW and 36.32W on a road of A-B class and E-F class respectively. The average power values of these kinds of road are 5.3mW and 1.67W respectively.

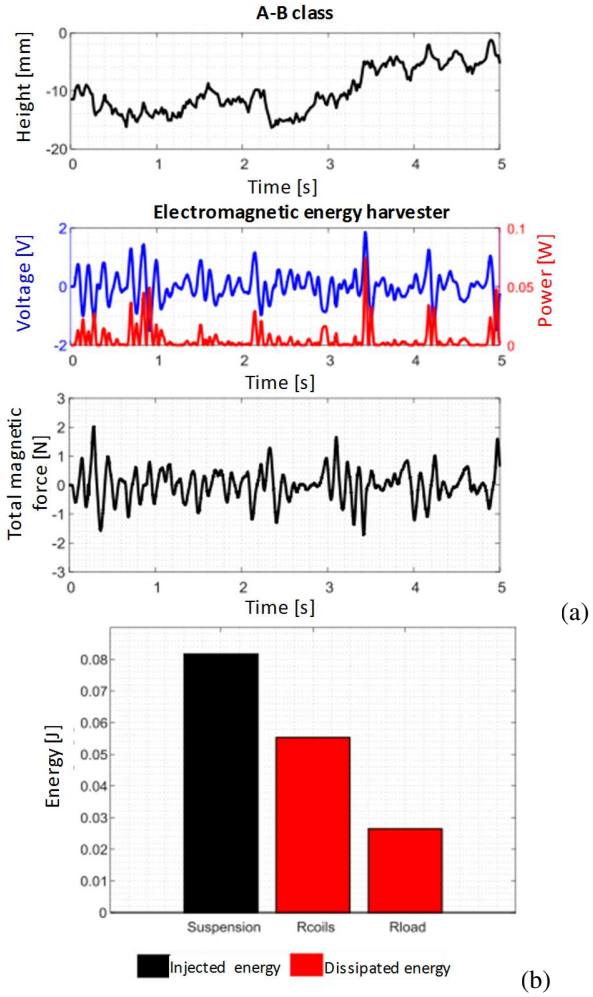

Fig. 18. Simulated voltages and powers with a load resistance value of 46.5Ω in case of driving through a class A-B road with a car speed of 20km/h (a) and evolution of the total injected energy (in black) and total dissipated energy (in red) for the electromagnetic energy harvester (b)

From the **Fig. 18-a**, it can be noted that the magnetic force is in the order of 2N. Therefore, the suspension dynamic behavior is relatively undisturbed for this class road and this car speed. As shown in **Fig. 18-b**, the simulated injected energy to the electromagnetic harvester by the suspension is equal to 81.71mJ. Once again, the mechanical energy is mainly dissipated in the coils (R_{coil}) and in the load (R_{load}) with 67.67% and 32.33% of the injected energy by the suspension respectively.

The E-F class coincides with a very poor surface with holes in the road pavement. The magnitude voltages and power are logically higher than in the previous case. The maximal power and the average power values are equal to 36.32W and 1.67W respectively. The magnetic force is also high with a maximal amplitude of 22.12N, but this force is low in comparison with the original suspension forces. Indeed, the suspension dynamic behavior is slighty disturbed due to the electromagnetic energy harvesters presence with a disturbance in order to 1% all over the vehicle.

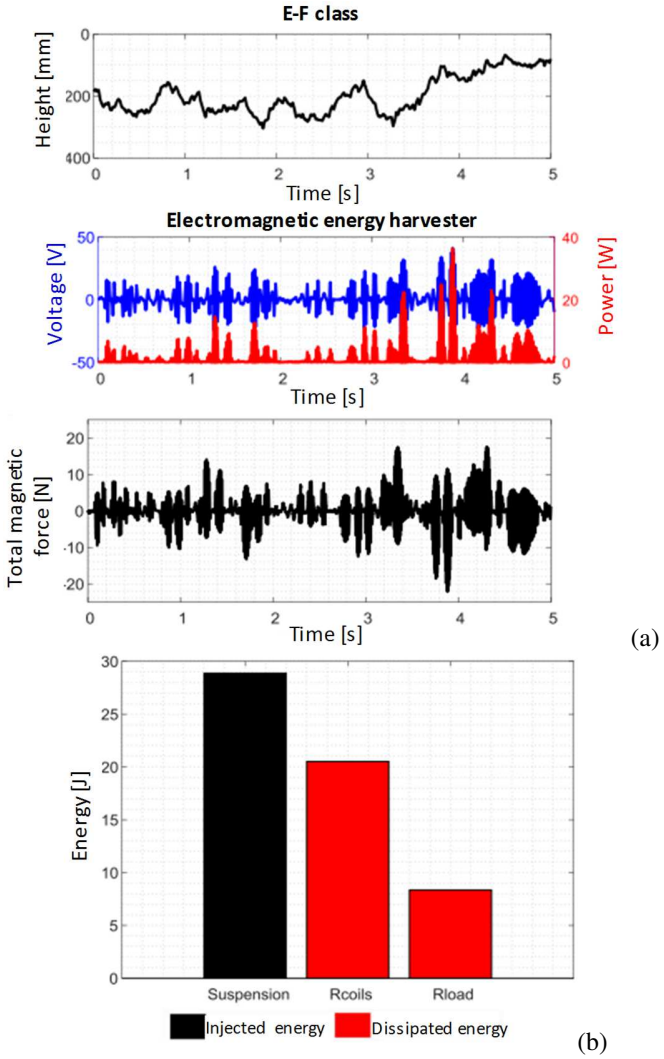

Fig. 19. Simulated voltages and powers with a load resistance value of 46.5Ω in case of driving through a class E-F road with a car speed of 20km/h (a) and evolution of the total injected energy (in black) and total dissipated energy (in red) for the electromagnetic energy harvester (b)

As shown in **Fig. 19-b**, the injected energy to the electromagnetic harvester by the suspension is equal to 28.86J. Once again, the mechanical energy is mainly dissipated in the coils (R_{coil}) in the load (R_{load}) with 71.10% and 28.92% of the injected energy by the suspension respectively.

When comparing the dissipated energies in the resistive load in the A-B and E-F class of the road pavement, a significant variation of 99.68% is observed. This result is coherent on roads from excellent to poor pavement. To conclude, according to the road classification, it is possible to supply either continuously or alternatively an auxiliary control circuit.

VI. CONCLUSION

In this paper, the study has been focused on the design and fabrication of a fully embedded linear electromagnetic harvester without changing the initial structure of the suspension. To enable an optimum design, it has been however necessary to propose a modeling method sufficient robust to evaluate the efficiency of the system.

In order to evaluate the electrical, mechanical and electromechanical parameter, a static finite element analysis has been first performed in a first step whereas in the second step, these linear and nonlinear parameters have been injected in a dynamic BG model to evaluate the efficiency of the system.

Dynamic tests have been then successfully performed and compared with simulation results for a solicitation of linear velocity of 0.75m/s and 1m/s. Obtained results are very promising since the embedded linear electromagnetic harvester system delivers around 10 watts which is enough to power a classical electronic circuit. In comparison with the performances of energy harvester systems embedded in a car suspension in **Fig. 1**, our harvester system delivers results close to the harvesters cited in references

LEH: linear electromagnetic energy harvester

[**4**], [**11**] and [**17**] with the particularity of being embedded in a classic car shock absorber without modifying the structure of the car.

In addition, a simulation of the complete system has been proposed with an analysis allowing extracting injected, stored and dissipated powers in both mechanical and electrical domains and for all subsystems as function of time and for the case of a speed bump solicitation. To our knowledge, this is the first time that a complete modeling (i.e. composed of the car suspension, the electromagnetic energy harvester and the restitution circuit) is proposed.

In view of an energy balance, significant average power is obtained since the simulated results give 4.4mW for a speed bump solicitation, and 5.3mW and 1.67W on a road of A-B class and E-F class respectively with an electromagnetic efficiency equal to $\eta = 0.2924$.

Future work is now in progress to test this system in real time on a car driven on a road.

REFERENCES

[1] M.A.A. Abdelkareem, L. Xu, M. Kamal Ahmed Ali, A. Elagouz, J. Mi, S. Guo, Y. Liu, L. Zuo, "Vibration energy harvesting in automotive suspension system: A detailed review", Applied Energy, Vol. 229, pp. 672-699, 2018

[2] B. Lafarge, S. Grondel, C. Delebarre, E. Cattan, "A validated simulation of energy harvesting with piezoelectric cantilever beams on a vehicle suspension using Bond Graph approach", Mechatronics, Vol. 53, pp 202-214, 2018

[3] B. Lafarge, S. Cagin, O. Curea, A. Hacala Perret, "From functional analysis to energy harvesting system design: application to car suspension", International Journal on Interactive Design and Manufacturing (IJIDeM), Vol. 10, pp. 37-50, 2016

[4] Y. Kawamoto, Y. Suda, H. Inoue, T. Kondo, "Modeling of electromagnetic damper for automobile suspension", Journal of System Design and Dynamics, Vol. 1, no. 3, pp. 524-535, 2007

[5] Z. Li, L. Zuo, J. Kuang, G. Luhrs, "Energy-harvesting shock absorber with a mechanical motion rectifier", Smart Materials and Structures, Vol. 22, no. 2, 2012

[6] Z. Li, L. Zuo, G. Luhrs, L. Lin, Y.-X. Qin, "Electromagnetic energy-harvesting shock absorbers: design, modeling, and road tests", IEEE Transactions on Vehicular technology, Vol. 62, no. 3, pp. 1065-1074, 2013

[7] Z. Zhang, X. Zhang, W. Chen, Y. Rasim, W. Salman, H. Pan, Y. Yuan, C. Wang, "A high-efficiency energy regenerative shock absorber using supercapacitors for renewable energy applications in range extended electric vehicle", Applied Energy, Vol. 178, pp. 177-188, 2016

[8] Y. Zhang, X. Zhang, M. Zhan, K. Guo, F. Zhao, Z. Liu, "Study on a novel hydraulic pumping regenerative suspension for vehicles", Journal of the Franklin Institute, Vol. 352, pp. 485-499, 2015

[9] R. Wang, F. Gu, R. Cattley, A.D. Ball, "Modelling, testing and analysis of a regenerative hydraulic shock absorber system", Energies, Vol. 9, no. 386, pp. 1-24, 2016

[10] Y. Zhang, H. Chen, K. Guo, X. Zhang, S.E. Li, "Electro-hydraulic damper for energy harvesting suspension: Modelling, prototyping and experimental validation", Applied Energy, Vol. 199, pp. 1-12, 2017

[11] Audit, "Innovative of the year: Audit eRot", VehicleDynamicsInternational.com, pp. 30, May/June 2017

[12] A. Gupta, J.A. Jendrzejczyk, J.M. Mulcahy, J.R. Hull, "Design of electromagnetic shock absorbers", Int. J. Mech. Mater. Des., Vol.3, pp. 285-291, 2006

[13] Z. Longxin, W. Xiaogang, "Structure and Performance Analysis of Regenerative Electromagnetic Shock Absorber", Journal of Networks, Vol. 5, no. 12, pp. 1464-1474, 2010

[14] L. Zhen, X. Wei, "Structure and Magnetic Field Analysis of Regenerative Electromagnetic Shock Absorber", 2010 WASE International Conference on Information Engineering, pp. 152-155, 2010

[15] X. Lin, Y. Bo, G. Xuexun, Y. Jun, "Simulation and performance evaluation of hydraulic transmission electromagnetic energy-regenerative active suspension", 2010 Second WRI Global Congress on Intelligent Systems, 2010

[16] L. Zuo, B. Scully, J. Shestani, Y. Zhou, "Design and characterization of an electromagnetic energy harvester for vehicle suspensions", Smart Materials and Structures, Vol.19, pp. 1-10, 2010

[17] B.L.J. Gysen, J.J.H. Paulides, J.L.G. Janssen, E.A. Lomonova, "Active electromagnetic suspension for improved vehicle dynamics", IEEE Transactions on Vehicular Technology, Vol. 59, no. 3, pp. 1156-1163, 2010

[18] C. Wei, H. Taghavifar, "A novel approach to energy harvesting from vehicle suspension system: Half-vehicle model", Energy, Vol. 134, pp. 279-288, 2017

[19] B. Ebrahimi, M.B. Khamesee, M.F. Golnaraghi, "Feasibility study of an electromagnetic shock absorber with position sensing capability", 34th Annual Conference of IEEE Industrial Electronics, pp. 2988-2991, 2008

LEH: linear electromagnetic energy harvester

[20] B. Ebrahimi, M.B. Khamesee, F. Golnaraghi, “Design of a hybrid electromagnetic/hydraulic damper for automotive suspension systems”, Proceedings of the 2009 IEEE International Conference on Mechatronics and Automation, August 9-12, Changchun, China, pp. 3196-3200, 2009

[21] E. Arroyo, A. Badel, F. Formosa, Y. Wu, J. Qiu, “Comparison of electromagnetic and piezoelectric vibration energy harvesters: Model and experiments”, Sensors and Actuators A: Physical, Vol. 183, pp. 148-156, 2012

[22] A. Munaz, B.-C. Lee, G.-S. Chung, “A study of an electromagnetic energy harvester using multi-pole magnet”, Sensors and Actuators A: Physical, Vol. 201, pp. 134-140, 2013

[23] S.-D. Kwon, J. Park, K. Law, “Electromagnetic energy harvester with repulsively stacked multilayer magnets for low frequency vibrations”, Smart Materials and Structures, Vol. 22, pp. 1-13, 2013

[24] G. Donoso, C.L. Ladera, P. Martin, “Magnet fall inside a conductive pipe: motion and the role of the pipe wall thickness”, European Journal of Physics, Vol. 30, pp. 855-869, 2009

[25] M.S. Soliman, E.M. Abdel-Rahman, E.F. El-Saadany, R.R. Mansour, “A wideband vibration-based energy harvester”, Journal of Micromechanics and Microengineering, Vol. 18, no. 11, pp. 1-26, 2008

[26] B.P. Mann, N.D. Sims, “On the performance and resonant frequency of electromagnetic induction energy harvesters”, Journal of Sound and Vibration, Vol. 329, no. 9, pp. 1348-1361, 2010

[27] E. Dallago, M. Marchesi, G. Venchi, “Analytical model of a vibrating electromagnetic harvester considering nonlinear effects”, IEEE Transactions on Power Electronics, Vol. 25, no. 8, 2010

[28] S. Priya, D.J. Inman, “Energy harvesting technologies”, Berlin: Springer, pp. 129-161, 2009

[29] P.K. Sinha, “Electromagnetic suspension: dynamics and control”, IEEE Control Engineering Series, Vol. 30, 1987

[30] D. Kumar, K. Chatterjee, “A review of conventional and advanced MPPT algorithms for wind energy systems”, Renewable and Sustainable Energy Reviews, Vol. 55, pp. 957-970, 2016

[31] T.J. Kaźmierski, S. Beeby, “Energy harvesting systems: Principles, modeling and applications”, Berlin: Springer, 2014

[32] E. Esmailzadeh, N. Jalili, “Vehicle-passenger-structure interaction of uniform bridges traversed by moving vehicles”, Journal of Sound and Vibration, Vol. 260, pp. 611-635, 2003

[33] G. Loprencipe, P. Zoccali, “Use of generated artificial road profiles in road roughness evaluation”, Journal of Modern Transportation, Vol. 25, no. 1, pp. 24–33, 2017